Journal of Rock Mechanics and Geotechnical Engineering 12 (2020) 449–460

Contents lists available at ScienceDirect

Journal of Rock Mechanics and Geotechnical Engineering

journal homepage: www.jrmge.cn

Full Length Article

Influence of location of large-scale asperity on shear strength of concrete-rock interface under eccentric load

Dipen Bista [a,b,*], Gabriel Sas [a], Fredrik Johansson [c], Leif Lia [b]

[a] SINTEF Narvik As, Narvik, 8517, Norway
[b] Norwegian University of Science and Technology (NTNU), Trondheim, 7491, Norway
[c] Royal Institute of Technology (KTH), Stockholm, 10044, Sweden

ARTICLE INFO

Article history:
Received 7 June 2019
Received in revised form
14 September 2019
Accepted 12 January 2020
Available online 12 May 2020

Keywords:
Shear strength
Concrete-rock interface
Asperity location
Eccentric load
Model discrepancy
Dam foundation

ABSTRACT

The location and geometry of large-scale asperity present at the foundation of concrete gravity dams and buttress dams affect the shear resistance of the concrete-rock interface. However, the parameters describing the frictional resistance of the interface usually do not account for these asperities. This could result in an underestimate of the peak shear strength, which leads to significantly conservative design for new dams or unnecessary stability enhancing measures for existing ones. The aim of this work was to investigate the effect of the location of first-order asperity on the peak shear strength of a concrete-rock interface under eccentric load and the model discrepancy associated with the commonly used rigid body methods for calculating the factor of safety (FS) against sliding. For this, a series of direct and eccentric shear tests under constant normal load (CNL) was carried out on concrete-rock samples. The peak shear strengths measured in the tests were compared in terms of asperity location and with the predicted values from analytical rigid body methods. The results showed that the large-scale asperity under eccentric load significantly affected the peak shear strength. Furthermore, unlike the conventional assumption of sliding or shear failure of an asperity in direct shear, under the effect of eccentric shear load, a tensile failure in the rock or in the concrete could occur, resulting in a lower shear strength compared with that of direct shear tests. These results could have important implications for assessment of the FS against sliding failure in the concrete-rock interface.

1. Introduction

The safety evaluation of existing concrete gravity dams or buttress dams is generally conducted by checking the safety of the dam using three different failure modes: sliding, overturning and overstressing. To evaluate the safety against sliding, the analytical rigid body methods, i.e. the shear friction method (SFM) and the limit equilibrium method (LEM), are commonly used (Nicholson, 1983; Krounis et al., 2015). The Mohr-Coulomb (MC) failure criterion is recommended in both the SFM and the LEM for calculating the peak shear strength (τ_{peak}) of the potential failure plane by most of the guidelines in practise for dams (ANCOLD, 1991; USACE, 1995; FERC, 2002; IS, 2003; NVE, 2005; USACE, 2005; CFBR, 2012; Canadian Dam Association, 2013; FERC, 2017). Sliding safety is generally evaluated for different potential failure planes, i.e. the dam foundation interface, the construction joints in the dam body, and the sub-horizontal rock joints in the dam foundation (CFBR, 2012). Among the guidelines mentioned above, FERC (2002), IS (2003), NVE (2005), and FERC (2017) use the SFM for sliding stability analysis.

In the SFM, failure is assumed along a plane, representing the average inclination of the sliding surface. The factor of safety (FS) is calculated as:

$$FS_{SFM} = T \Big/ \sum H \tag{1}$$

where T is the shear capacity of the sliding plane and $\sum H$ is the sum of forces parallel to the sliding plane, and T can be written as

$$T = cA + \sum N' \tan \phi \tag{2}$$

* Corresponding author.
E-mail address: dipen.bista@norut.no (D. Bista).
Peer review under responsibility of Institute of Rock and Soil Mechanics, Chinese Academy of Sciences.

https://doi.org/10.1016/j.jrmge.2020.01.001

where $\sum N'$ is the sum of effective forces normal to the sliding plane, ϕ is the friction angle, c is the cohesion, and A is the area of the sliding plane.

To calculate the FS with the LEM, the sliding plane can be divided into different sections (slip surfaces):

$$FS_{\mathrm{LEM}} = \tau_{\mathrm{R}}/\tau \tag{3}$$

where τ_{R} and τ are the available shear stress and resultant shear stress required for equilibrium, respectively. τ_{R} is defined by the MC criterion as

$$\tau_{\mathrm{R}} = c + \sigma'_{\mathrm{n}} \tan\phi \tag{4}$$

where σ'_{n} is the effective normal stress.

The MC failure criterion is widely used due to its simplicity and ease of use. However, in derivation of the parameters in this criterion, the local variations of geometry at the interface and its location, or the elastic deformations of materials, are not directly considered. These are indirectly built into the criterion as average values of cohesion and friction parameters representing the overall surface. These values are normally obtained by carrying out laboratory or in situ shear tests or from recommended values in guidelines. However, these parameters also vary spatially within the dam foundation interface. For example, Altarejos-García et al. (2015) and Krounis et al. (2015) showed that the FS can vary significantly when taking into account the spatial variability compared with a homogeneous interface using the same average values of these parameters. Furthermore, the value of the cohesion is difficult to obtain for a dam foundation, because of its spatial variability and dependence on a number of unknowns, such as surface preparation, loading history, surface degradation, and joints' roughness characteristics (Krounis et al., 2016; Mouzannar et al., 2017). Hence, cohesion is usually ignored, or a larger FS is used if cohesion is considered in rigid body analysis of dams (ICOLD, 2004).

A dam foundation interface is normally prepared by removing a top layer of rock by blasting. Hence, the rock surface can have roughness at different scales and amplitudes compared with rock joints. An example of this from a plate dam in Norway is illustrated in Fig. 1a. The large asperities are called first-order roughness or waviness (in metre- or decimetre-scale), and smaller asperities are called second-order roughness or unevenness (in centimetre- or millimetre-scale) (Patton, 1966). For a blasted surface, these large-scale asperities are usually highly irregular with large amplitude and large asperity inclinations, α, against the shear direction (see Fig. 1b). Laboratory and in situ tests fail to represent the dam foundation geometry because of scale difference between the sample and the large-scale irregularities at the dam foundation interface. Hence, the τ_{peak} obtained from laboratory only represents the second-order roughness and does not capture the effect of large-scale asperity at the decimetre- or metre-scale (Barton, 1978). However, the large-scale asperities present in the interface are normally those determining the overall behaviour of an interface (Patton, 1966; Grasselli, 2001; Asadi et al., 2013; Gravel et al., 2015; Zhang et al., 2016).

In order to better access the uncertainties associated with different parameters included in stability analysis of dams, reliability-based analyses have generally been used (e.g. Wilde and Johansson, 2013, 2016; Altarejos-García et al., 2015; Bernier et al., 2016). However, even though reliability-based analyses account for the variability of the parameters compared to deterministic methods, the acceptance level for the probability of failure of dams is still debatable (Altarejos-García et al., 2015). The deterministic methods of FS assessment are still popular and commonly used for the safety evaluation of dams (ICOLD, 2004; Donnelly, 2007).

Several criteria have been developed over the years to calculate the τ_{peak} of joints based on empirical methods (e.g. Schneider, 1976; Barton and Choubey, 1977; Maksimović, 1996; Yang et al., 2016; Zhang et al., 2016), fractal methods (e.g. Brown and Scholz, 1985; Huang et al., 1992; Odling, 1994; Kulatilake et al., 1995; Den Outer et al., 1995; Kulatilake et al., 2006), energy and work principles (e.g. Ladanyi and Archambault, 1970; Plesha, 1987; Li et al., 2015; Oh et al., 2015), and quantified surface description (e.g. Grasselli, 2006; Johansson and Stille, 2014; Xia et al., 2014). The main aim of these criteria is to quantify the natural roughness of the rock surface and these works are mostly based on laboratory-scale samples. Only second-order roughness of the concrete-rock interface of a dam foundation is represented by these criteria. Hencher and Richards (2015) proposed a method for estimating the shear strength at project-scale using dilation-corrected basic friction angle and considering the contribution of roughness at multi-scale. The contribution of large-scale roughness was calculated by adjusting the friction angle for the dip of the large-scale roughness assuming a sliding failure over the large-scale. However, for dams where the artificially prepared surface may have high angle first-order

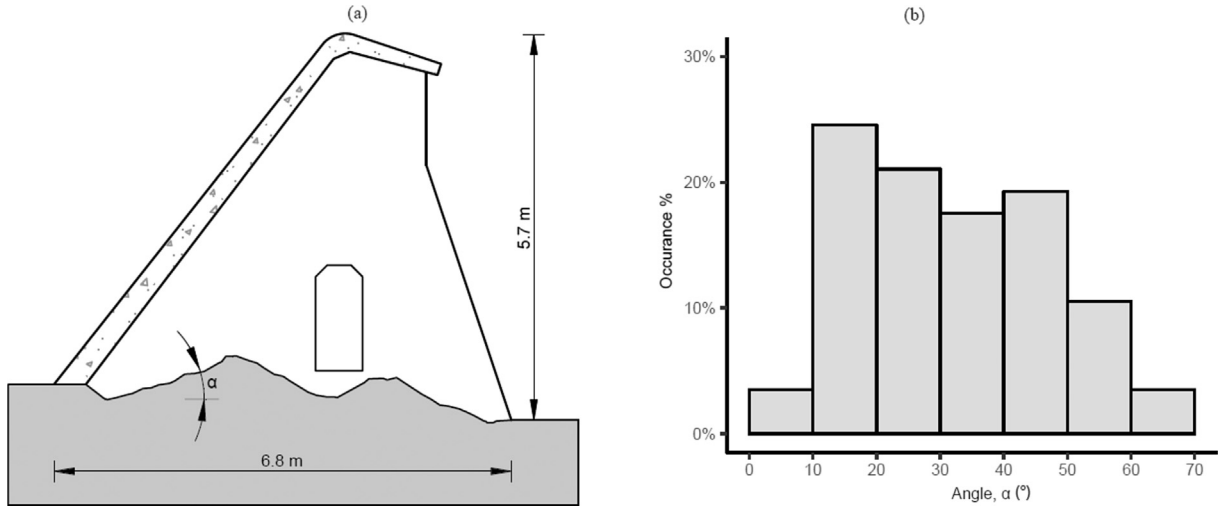

Fig. 1. (a) Example of first-order roughness and (b) Distribution of front leg angle of first-order asperity with length greater than 10% of dam height from Kalhovd dam in Norway.

asperities (see Fig. 1), failure modes other than sliding over the asperity need to be considered. Furthermore, the above-mentioned criteria are basically based on pure shear load on the samples assuming a constant normal stress. However, the resultant force applied on the dam usually falls downstream of the interface centroid resulting in a moment by stresses. This is defined as eccentric load in this paper, which creates an uneven distribution of normal stress at the interface, with higher normal stresses at the downstream side and lower ones at the upstream side.

Fishman (2008) investigated the failure mechanism under compressive shear load. Tests were carried out on blocks of continuous material and blocks with bonded and unbonded block-foundation interface. Fishman (2008) concluded that under compressive shear load, over a certain normal stress value, the failure initiates through a primary tensile crack, followed by a compressive crack. Furthermore, the unbonded interface acts as a single unit above a certain normal stress. However, this criterion does not take into account to what extent the asperity on the interface contributes to the τ_{peak}.

Since the normal stress in a dam varies along the interface because of an eccentric load, the asperities at different locations are subjected to different levels of normal stresses. This may result in different failure modes of the asperities; hence, asperities at different locations contribute differently to the τ_{peak}. However, the effect of the location of first-order asperity on the τ_{peak} under eccentric load has not been reported yet to date.

The aim of this study is to investigate the effect of the location of first-order asperity on the τ_{peak} and the mode by which asperity fails under eccentric load compared to direct shear with a constant normal stress. The paper also investigates the potential model discrepancy associated with the commonly used rigid body methods for sliding stability when the asperity is not considered. A series of direct shear tests and eccentric shear tests (i.e. shear tests subjected to an eccentric load) was carried out on concrete-rock joints with asperities at different locations. A monitoring system based on digital image correlation (DIC) was used to record full-field measurements for the samples. The results were analysed with respect to the location of asperity and thereafter compared with predicted values from analytical rigid body methods. Based on these results, the failure mode of asperity and its contribution to the τ_{peak}, together with the model discrepancies and potential implications for dam safety, were discussed.

2. Laboratory shear test

2.1. Experimental programme

In order to investigate the effect of asperity location on the τ_{peak} under direct load and eccentric load, a series of concrete-rock samples with size of 280 mm × 270 mm × 130 mm (length × width × thickness) was prepared. The samples having a symmetric triangular shaped asperity of 60 mm length and 45° angle (height of asperity of 30 mm) at the front, middle, and end are shown in Fig. 2. Three asperity locations were chosen because the normal stress acting at the front, middle, and end will be the lowest, median, and highest under eccentric load, respectively. A total of 22 samples were tested under two different types of loadings: (a) direct shear and (b) eccentric shear (see Section 2.4). Four samples without asperities, two for each loading scenario, were also tested to serve as a reference to those samples with an asperity. The samples were tested under three different normal stresses, i.e. 0.2 MPa, 0.6 MPa and 1.0 MPa. These normal stresses were selected based on the maximum normal stresses acting on the upstream and downstream sides of a plate/buttress dam with a height of 2–15 m. A summary of the shear test programme is given in Table 1. A unique identity was created for each sample. The first letter refers to the loading set-up (direct shear test = D, eccentric shear test = E), the second letter refers to the location of asperity in the sample (no asperity = N, front = F, middle = M, end = E), and the number at the end refers to the normal pressure (MPa) applied to the sample. For example, a sample with an identity DE0.6 would read the one used for direct shear test, with asperity at its end and normal pressure of 0.6 MPa applied to the sample during the test.

2.2. Sample selection

For simplicity, a regular triangular-shaped asperity was chosen. A 45° angle was selected for the tests with two main reasons: (1) the angle of the asperity was corresponding to those observed in field where the surface was prepared by blasting (Fig. 1b); (2) for test series, the objective was to compare the results of direct shear and eccentric shear tests. Under direct shearing scenarios, a sample with a low angle asperity (<30°) normally fails due to sliding over the asperity (Johansson, 2009; Liahagen et al., 2012). The contribution of asperity to the shear strength will be less when it fails at sliding over the asperity. Hence, it was hypothesized that, a high angled asperity could give a greater difference between the direct shear and eccentric shear tests. Therefore, an angle of 45° was chosen for the test.

2.3. Sample preparation

The granite samples were extracted from a quarry and prepared by sawing into specified dimensions. The compressive strength of the rock was determined by compression tests on six cylindrical rock cores as per ASTM D7012-14 (2014). Similarly, the tensile strength of the rock was determined by splitting tests on ten samples as per ASTM D3967-16 (2016). The rock used for the tests

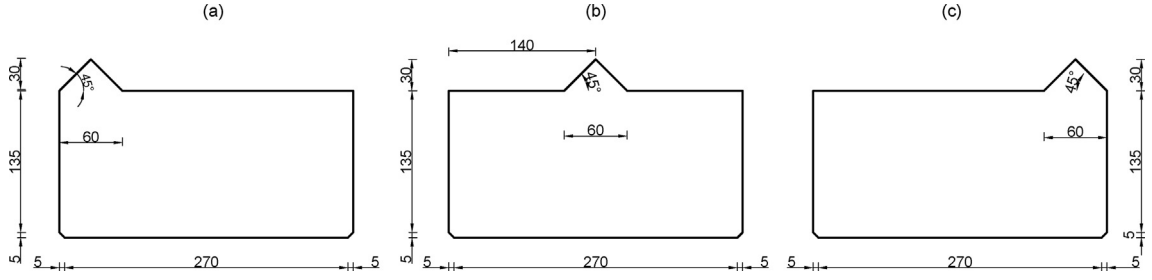

Fig. 2. Detail dimensions of samples (mm): (a) Asperity at the front, (b) Asperity in the middle, and (c) Asperity at the end.

Table 1
Summary of shear tests.

Test	No asperity		Front			Middle			End		
Direct shear	DN1.0	DN0.6	DF1.0	DF0.6	DF0.2	DM1.0	DM0.6	DM0.2	DE1.0	DE0.6	DE0.2
Eccentric shear	EN1.0	EN0.6	EF1.0	EF0.6	EF0.2	EM1.0	EM0.6	EM0.2	EE1.0	EE0.6	EE0.2

had an average uniaxial compressive strength (σ_{ci}) of 181 MPa and an average tensile strength (σ_{ti}) of 13.5 MPa. A thin layer of rubber spray paint was applied on the rock surface to prevent it from bonding with concrete (see Fig. 3a). It was found that the rubber paint effectively prevented bonding between rock and concrete and gave the best surface representation of rock on concrete from the materials tested. The rubber paint that was sprayed over the rock surface developed into a thin film upon drying. Prior to testing, the rubber paint was peeled off the rock surface by hand.

The rock samples were then placed in steel formworks (see Fig. 3b) and the concrete was cast over the surface. Compression tests on 12 concrete cylinders were carried out as per ASTM C39/C39M-17 (2017). The concrete used in the test had an average characteristic cylindrical strength of 25.8 MPa after 28 d. The samples were then cured in water for 28 d.

2.4. Test set-up and loading strategy

Two different loading set-ups were used for the test: direct shear test under constant normal load (CNL) and eccentric shear test under CNL. The normal load was applied to the samples continuously at a constant rate of 0.01 MPa/s as specified in Muralha et al. (2014).

2.4.1. Direct shear test

The shear testing machine at Luleå University of Technology (LTU) was designed for direct shear tests at CNL as described by Johansson (2009), and among others (see Figs. 4 and 5a). The machine is capable of carrying out shear tests on samples with side length up to 280 mm, in accordance with the International Society for Rock Mechanics (ISRM) suggested method given by Muralha et al. (2014). The lower shear box was fixed while the upper one could translate on a horizontal plane when shear load was applied. During the direct shear test, samples were sheared at a constant rate of 0.5 mm/min. This low shear rate was chosen to avoid uncontrolled failure and excess displacements in the sample.

2.4.2. Eccentric shear test

The shear box used for the direct shear tests was modified to apply an eccentric shear load. An iron strip with thickness of 8 mm and width of 30 mm was mounted on the inner side of the upper shear box. The centre of the strip was located 100 mm above the concrete-rock interface (see Fig. 5b). A shear load was applied on the shear box with a hydraulically controlled external load cell mounted on the steel frame. The load cell was mounted at the same height as the iron strip over the interface. This set-up allows the top concrete to rotate if there is any rotation induced by the eccentric shear force while keeping the rock on the lower shear box fixed.

2.5. Instrumentation

Two optical measurement systems, based on DIC, ARAMIS (GOM GmbH, 2017a) and GOM Snap 2D (GOM GmbH, 2017b), were used to monitor and record the testing data. A stochastic point pattern was created by spraying paint onto one side of the sample while a stochastic black dot pattern was created on the shear box using a stencil. ARAMIS was used to monitor the area around the asperity while GOM Snap 2D was used to monitor the overall sample and the movements of the shear box. The data from ARAMIS and GOM Snap 2D were processed and analysed with GOM Correlate Professional (GOM GmbH, 2018).

In addition to the DIC systems, linear variable differential transformers (LVDTs) were also used for monitoring the movement of the shear box. Furthermore, video recordings and still pictures were taken to supplement these measurements.

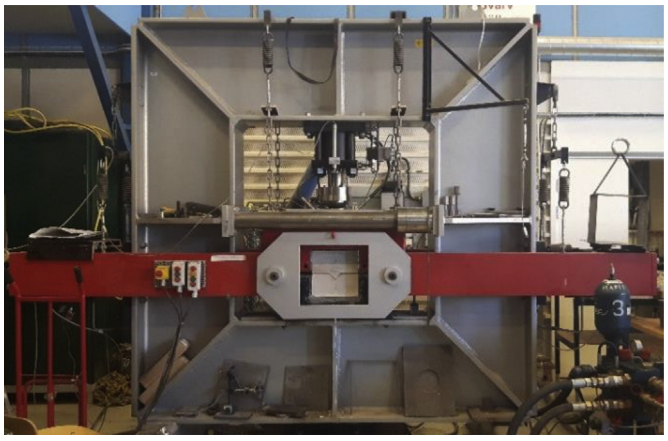

Fig. 4. Luleå University of Technology's direct shear machine.

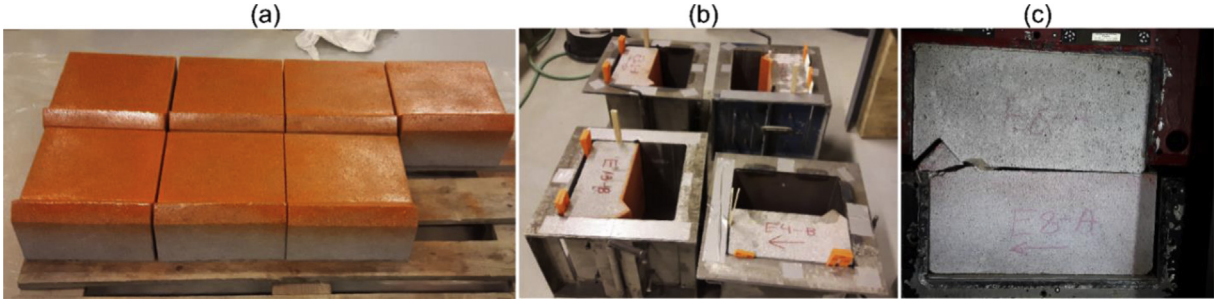

Fig. 3. (a) Applying rubber paint to prevent bonding, (b) Placement of samples in formworks, and (c) Samples under direct shear test.

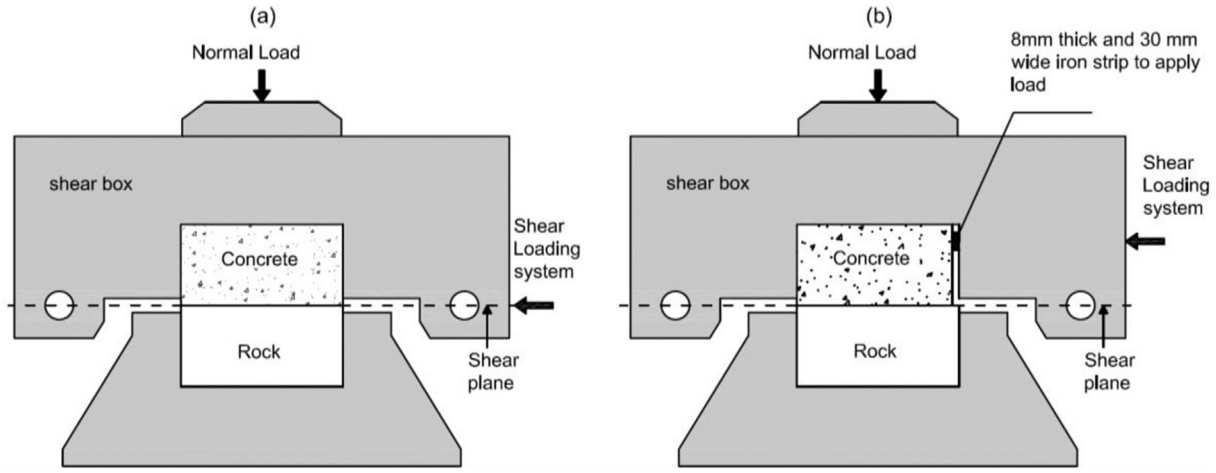

Fig. 5. Schematic diagram of loading set-up for (a) Direct shear test and (b) Eccentric shear test.

3. Results

A summary of the results obtained from the tests is shown in Fig. 6. The shear rate applied in the sample DM0.6 was set 10 times higher than the planned due to an error on the piston control, leading to uncontrolled shear behaviour of this sample. Hence sample DM0.6 has been excluded from the results.

3.1. Tests with no asperity

The samples with no asperity failed by sliding over the interface. No differences in failure mode and strength were observed between direct shear and eccentric shear tests for these samples (see Fig. 6). These tests were used to determine the basic friction angle (ϕ_b) of the concrete-rock samples, which was found to be 39.3°. This value is similar to the suggested ϕ_b for concrete-rock joints by Wilde and Johansson (2016).

3.2. Direct shear test

A summary of the results obtained from the direct shear tests is shown in Fig. 6a. For the samples with asperity, the highest τ_{peak} of 2.7 MPa was obtained with a normal pressure of 1.0 MPa and the lowest τ_{peak} of 0.9 MPa was obtained at 0.2 MPa normal pressure.

The progression of the tests can be described as follows. Initially, when the shear load was applied, the concrete slightly slid over the rock asperity. This opened up the contact between the concrete and the rock blocks at all the interfaces, except at the front leg of the asperity, which then undertook the entire normal load applied. As the shear load further increased, a tensile crack developed from the base of the asperity and progressed below the asperity. In Fig. 7, it can be observed that the cracks in the samples at the peak shear load occurred in the areas where the major strain (ε_1) reached its maximum of approximately 1.5% (shown in red colour in the figure). The major strain on the surface of the samples shown in Figs. 7 and 8 was plotted by measuring the deformation of random points on the surface of the samples by ARAMIS (GOM GmbH, 2017a). The development of this tensile crack is similar to that by Fishman (2008) under compressive shear load. Cracks were seen in the concrete between the asperity and the shear box prior to τ_{peak}, for samples with the asperity at the front and middle. However, the shear capacity decreased only when cracks appeared in the rock asperity because the concrete that cracked before reaching τ_{peak} was confined in the shear box. This allowed the concrete to take the load even after cracking.

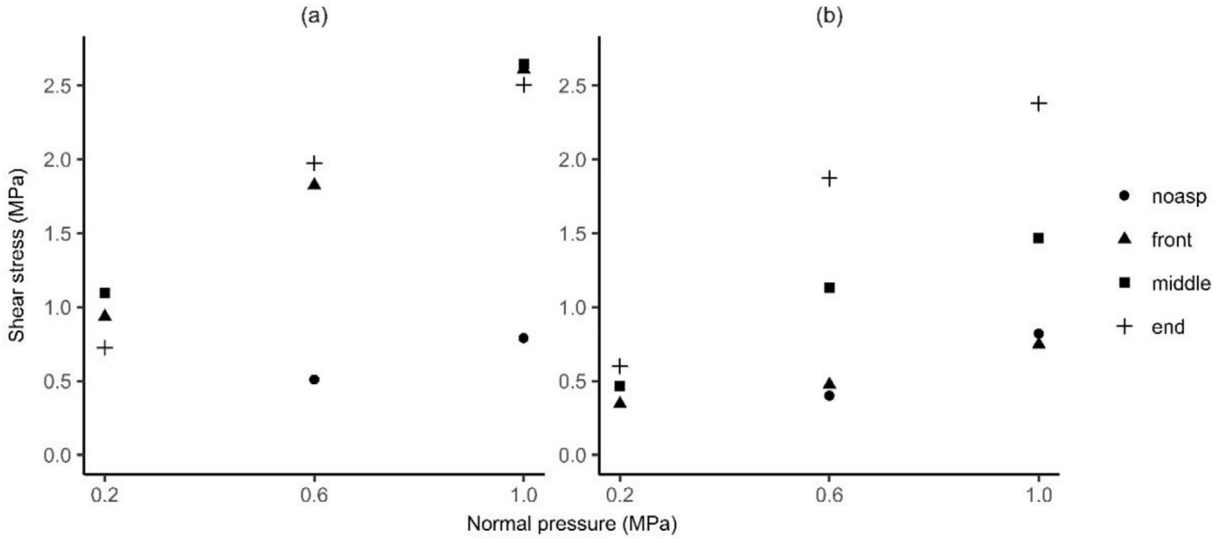

Fig. 6. Results of laboratory shear tests: (a) Direct shear tests, and (b) Eccentric shear tests. noasp means no asperity in the samples.

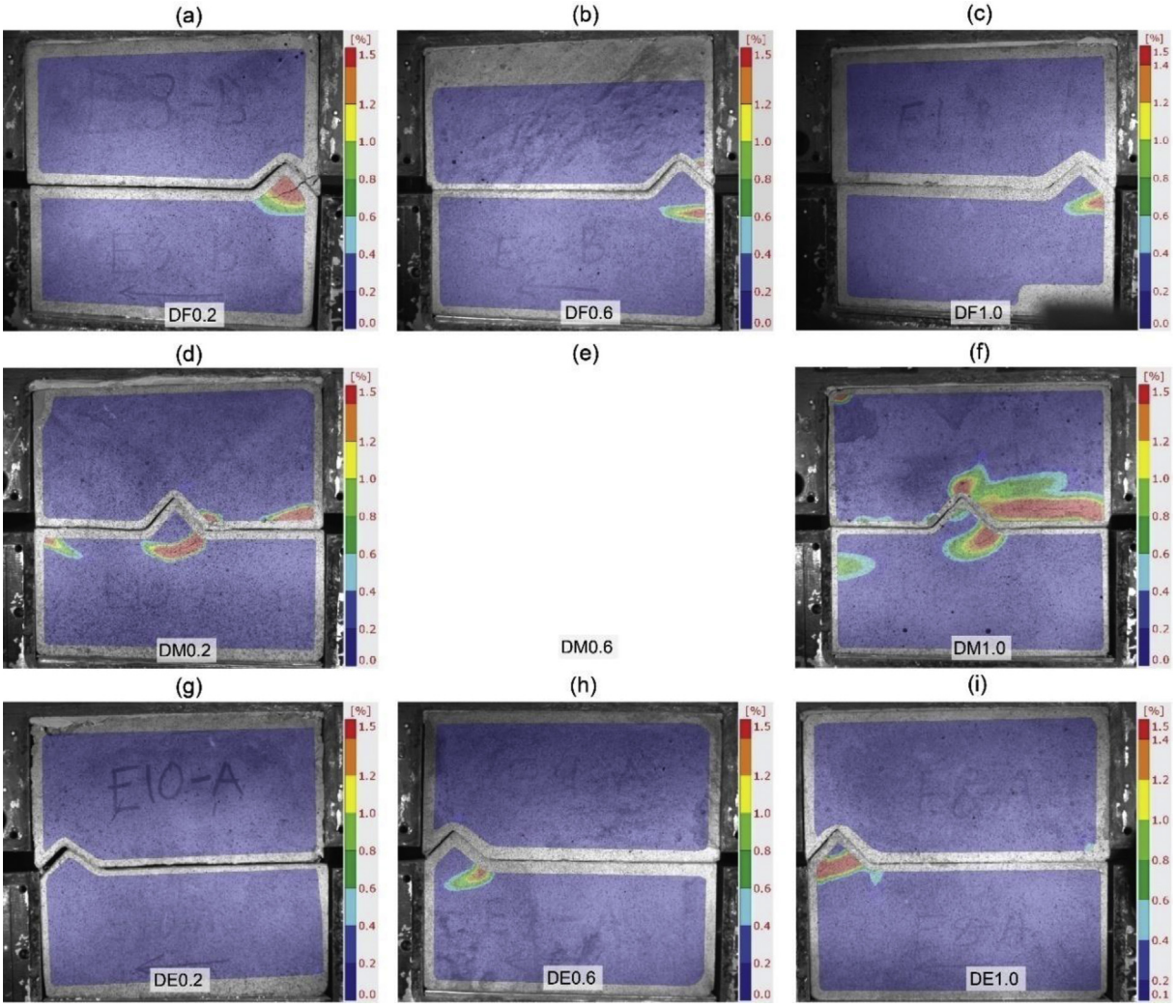

Fig. 7. Major strain (ε_1) plot of samples in direct shear tests (for all samples, the loading direction is from right to left). The red colour shows areas with higher strains. Sample DM0.6 has been excluded due to an error on the piston control.

From the direct shear tests, it was seen that there was no effect caused by the location of the asperity (see Fig. 6a). The reason for this is that the direct shear test set-up only allows a translation in the horizontal direction of the upper shear box and does not allow free rotation of the top concrete. This results in similar normal stresses on the asperity for all the locations of the asperity. Hence, a similar failure mechanism of the asperity was observed for all the samples in the direct shear tests, suggesting that the failure mechanism was not affected by asperity location for these samples (see Fig. 6). This is also apparent from the MC parameters, which were derived based on a linear best fit of the test results under different normal stresses. The MC parameters show similar values of cohesion and friction angle for all the locations of asperity (see Table 2). Hence, it can be concluded that the MC parameters obtained from direct shear tests are not influenced by the location of asperity. Failure through the rock asperity was observed for all the samples except DE0.2. The recorded τ_{peak} of the sample DE0.2 corresponded to sliding of the concrete over the rock asperity. The ultimate failure of sample DE0.2 occurred when shearing through approximately 1/3 of the asperity, while the remaining part remained intact (see Fig. 7g).

3.3. Eccentric shear test

A summary of the results obtained from the eccentric shear tests is shown in Fig. 6b. From the results, it was seen that the location of the asperity significantly affected the τ_{peak} of the samples. The highest τ_{peak} of 2.4 MPa was obtained for the sample with asperity at the end under normal pressure of 1.0 MPa and the lowest τ_{peak} of 0.4 MPa for the sample with asperity at the front under normal pressure of 0.2 MPa.

For all the samples, as the shear load was applied, the concrete slid up the asperity by a small distance and the contact at the rear leg of the asperity opened up (see Fig. 8). When the eccentric shear force was applied, the normal force was redistributed, with the lowest normal stress at the loading side and the highest at the opposite. With further application of shear load, a part of the interface towards the loading side opened up (for samples with asperity at the middle and the end) and the normal stress was further redistributed, resulting in higher normal stress at the end.

In the samples with asperity at the front (see Fig. 8a–c), a tensile crack developed in the concrete from the asperity tip and progressed towards the loading point. τ_{peak} occurred when the crack

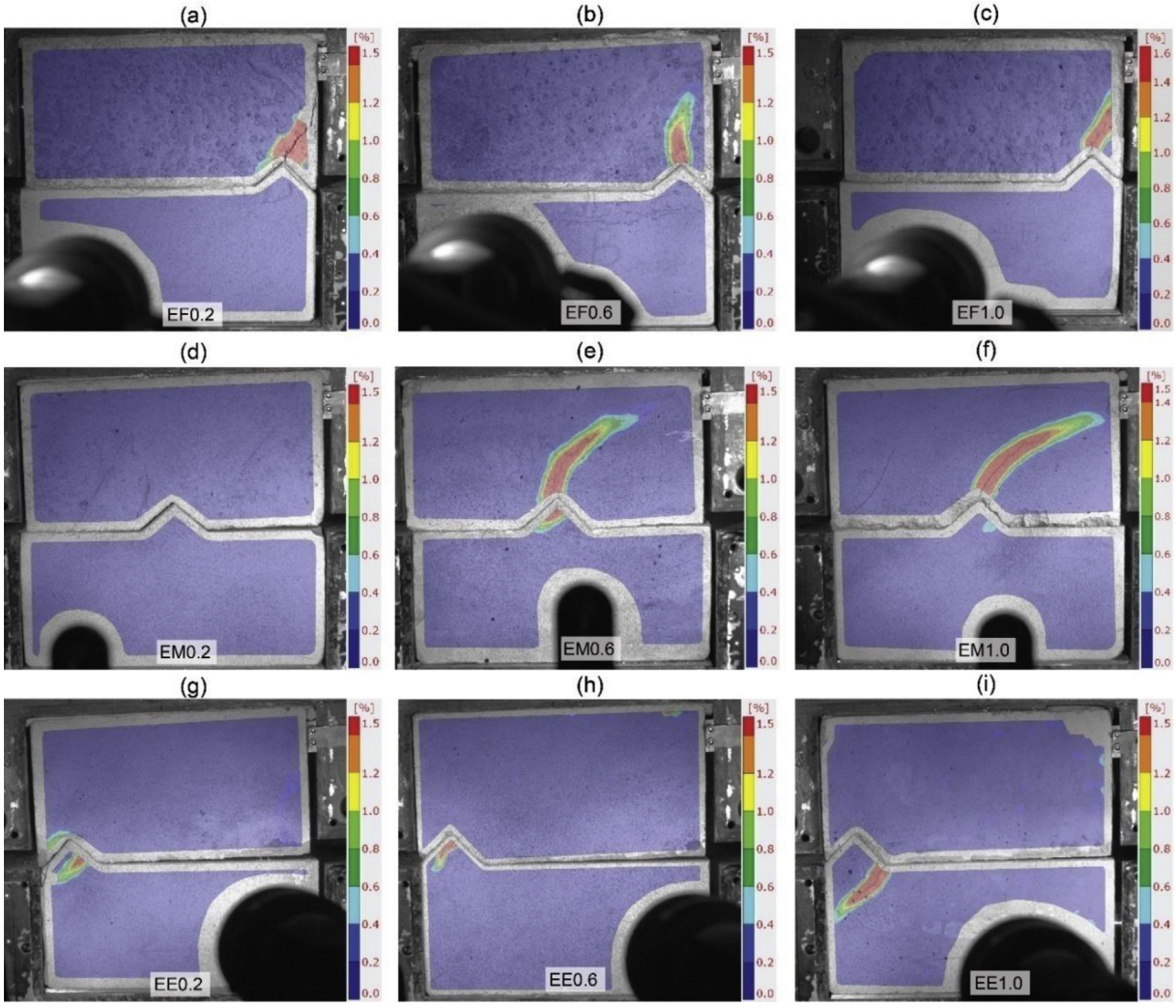

Fig. 8. Major strain (ε_1) plot of samples in eccentric shear tests (for all samples, the loading direction is from right to left).

started, and the shear strength thereafter decreased continuously as the crack propagated.

In the samples with asperity at the middle (see Fig. 8d–f), the top concrete rotated with the point of rotation approximately located at the asperity end. Hence, at τ_{peak}, no contact between concrete and rock was observed at the flat interface in front of the asperity towards the loading side while the interface behind the asperity was in contact. These samples failed by cracking of concrete between the asperity and the loading point. Furthermore, in the samples with asperities at the end (see Fig. 8g–i), similar to the samples with asperity at the middle, rotation of the concrete was observed approximately on the asperity end. At τ_{peak}, no contact between concrete and rock was observed at the flat interface in front of the asperity and the applied load was resisted by the asperity alone. A tensile crack started in the rock at the asperity base and progressed below the asperity. The failure mechanism of these samples was similar to that of samples under direct shear tests.

Under eccentric shear test, the failure mode of the samples varied for different locations of asperity. Furthermore, the area of the rock-concrete interface in contact was different for different locations of asperity. This resulted in an increase in the friction angle with increasing distance of the asperity from the front of the sample, while the cohesion remained fairly constant for all the locations of the asperity (see Table 2). This variation in the MC parameters with asperity location clearly shows that the asperity location under eccentric load has a significant influence on the τ_{peak}.

Table 2
Mohr-Coulomb parameters calculated for the laboratory samples.

Asperity	Direct shear test		Eccentric shear test	
	c (MPa)	ϕ (°)	c (MPa)	ϕ (°)
No	0.08	35.2	−0.22	46.1
Front	0.54	64.5	0.22	26.7
Middle	0.71	62.7	0.27	51.6
End	0.4	65.8	0.28	65.8

4. Discussion

4.1. Effect of location of asperity under eccentric load

Under an eccentric shear load, τ_{peak} of samples with an asperity at the end was about 3–4.5 times higher than that of samples without an asperity at the same normal pressures. The τ_{peak} of samples with an asperity at the middle was about 1.8–2.8 times

higher than that of samples without an asperity. On the other hand, the sample with an asperity at the front had a similar τ_{peak} as the one without an asperity. Thus, it can be concluded that the location of asperity under eccentric load significantly affects the τ_{peak}.

In the samples under eccentric shear load with an asperity at the end, due to the moment induced by the load, only the front leg of the asperity was in contact (see Fig. 8g–i). No clear shear failure of the asperity was observed in the samples. A tensile crack started at the base of the asperity and the failure occurred by opening of this crack and rotation of the sample at the asperity end. This failure mechanism is similar to that reported by Fishman (2008).

In order to illustrate the failure mode and calculate the shear strength of the sample with an asperity at the end, stress distribution due to normal and shear stresses were assumed, as shown in Fig. 9. Shear resistance from three individual failure modes of the asperity was calculated using the method as described by Johansson and Stille (2014), i.e. sliding failure over the asperity, shear failure of the asperity through its base, and tensile failure of the asperity.

For sliding failure over the asperity, the peak shear load, $T_{sliding}$, is calculated using the criterion by Patton (1966):

$$T_{sliding} = N\tan(\phi_b + i) \tag{5}$$

where N is the normal load applied, and i is the angle of asperity.

For a shear failure through the base of asperity, the peak shear load, T_{shear}, is calculated with the MC criterion:

$$T_{shear} = c_i w L_{asp} + N\tan(\phi_i) \tag{6}$$

where c_i and ϕ_i are the cohesion and internal friction angle of intact rock, respectively; w is the width of asperity; and L_{asp} is the length of asperity.

Tensile failure of the asperity will start at the base of asperity towards the loading side when (Johansson and Stille, 2014)

$$\sigma_t - \sigma_c = \sigma_{ti} \tag{7}$$

where σ_t is the tensile stress due to the resulting moment, ΣM, caused by N and T; σ_c is the average compressive stress due to normal load N; and σ_{ti} is the tensile strength of the rock. Since the samples are only in contact at the front leg of the asperity, the normal stress, σ_c, is assumed to be distributed only in the projected area of the front leg of the asperity. The resulting tensile stress at the front of the asperity due to ΣM can be calculated according to classical beam theory. Hence, Eq. (7) can be written as (note that tensile stress is defined as positive and compressive stress as negative):

$$\sigma_{ti} = \frac{\sum M}{I}\frac{L_{asp}}{4} - \frac{N}{0.5L_{asp}w} \tag{8}$$

where

$$\sum M = T_{tensile}h - N\left(\frac{L}{2} - \frac{3}{4}L_{asp}\right) \tag{9}$$

$$I = \frac{wL_{asp}^3}{12} \tag{10}$$

where I is the inertia moment of the base of asperity, h is the eccentricity of the resultant shear load, and L is the length of the sample.

Combining Eqs. (8) and (9), $T_{tensile}$ gives

$$T_{tensile} = \frac{\left(\sigma_{ti} + \frac{N}{0.5L_{asp}w}\right)\frac{4I}{L_{asp}} + N\left(\frac{L}{2} - \frac{3}{4}L_{asp}\right)}{h} \tag{11}$$

where $T_{tensile}$ is the peak shear load against tensile failure.

The smallest shear resistance calculated by Eqs. (5), (6) and (11) will govern the failure mode of the asperity. The results from this calculation will be referred to as 'asperity model' in this paper. ϕ_b of 39.3° and σ_{ti} of 13.5 MPa were used for calculation, which were obtained from laboratory tests. The value of cohesion for the intact rock 'c_i' was taken twice the σ_{ti}, i.e. 27 MPa, based on the Griffith theory of fracture (Brace, 1960), and ϕ_i of 68° was chosen (Stowe, 1969; Lanaro and Fredriksson, 2005) for the intact rock. 'h' was measured from the rock concrete interface to the middle of the loading iron strip, which was 100 mm (see Fig. 5b).

For the eccentric shear tests with an asperity at the end, Eq. (11), i.e. the tensile failure of the asperity, gave τ_{peak} closest to the values observed in the tests (see Fig. 10). Even though the model used to calculate $T_{tensile}$ was based only on an approximation of the true stress state in the asperity, the results are in agreement with the failure mode observed in the test, where a tensile failure mode was observed.

In a direct shear test, the shear load theoretically acts on the interface. However, due to practical limitations in a test set-up, some eccentricity of the shear load is expected. Since the eccentricity of shear load in the direct shear test set-up is unknown, an analytical calculation of tests under direct shear by the asperity model is not performed.

For samples under eccentric shear tests, with the asperity at the front or middle, the stress was redistributed among the surfaces in contact, i.e. the front leg of asperity and the flat interface behind the asperity. The accurate estimate of redistributed stress is a complex process that requires advanced numerical calculations (Haberfield and Johnston, 1994). Therefore, calculations with the asperity model were not performed for these models, and the variation of τ_{peak} for these samples was only explained qualitatively.

For samples under eccentric shear tests, with an asperity at the front (see Fig. 8a–c), failure occurred due to tensile failure in the concrete, which started at the asperity tip and progressed towards the loading point. Hence, the shear resistance was provided by the tensile strength of the concrete between the asperity and the shear

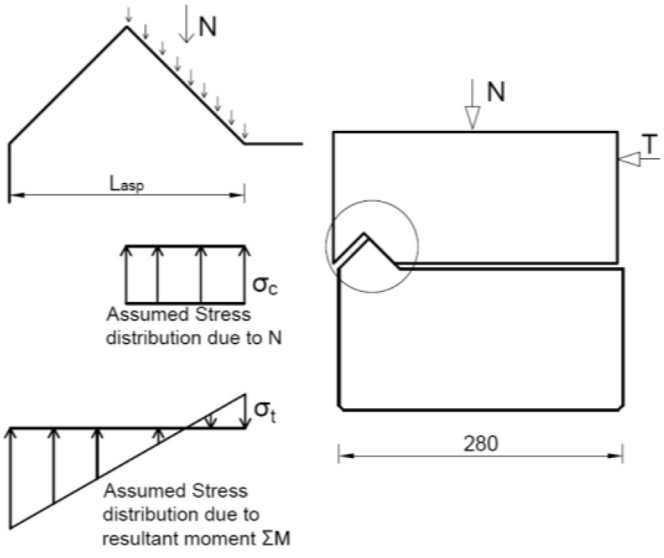

Fig. 9. Assumed stress distribution due to normal load (N) and shear load (T) for a sample with an asperity at the end. Dimension is in mm.

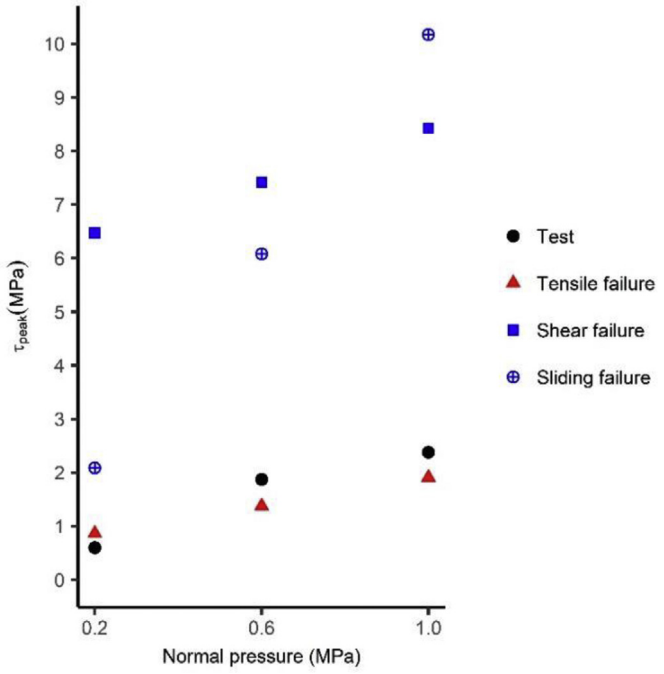

Fig. 10. Comparison between test results and the estimated τ_{peak} from the asperity model for samples with an asperity at the end under eccentric shear load.

box and the frictional resistance between the concrete and the rock behind the asperity. Furthermore, as concrete is weak in tension and the length of the failure surface through the concrete is small, only a small percentage of the total resistance is provided by the concrete, with a greater part mobilised by the friction between the concrete and rock. Therefore, the resistance provided by these samples was less compared to samples with the asperity at the middle and the end.

For the samples with the asperity at the middle (see Fig. 8d–f), since the contact between concrete and rock opened up at the flat interface in front of the asperity, the shear load was resisted by the rock asperity and by frictional resistance at the flat interface after the asperity. The samples failed for the development of crack in the concrete between the asperity and the loading point, and a crack at the rock asperity also appeared simultaneously (see Fig. 8e,f). It could not be detected which failure occurred corresponding to the τ_{peak}. However, as the length of crack in concrete was longer than that of samples with the asperity at the front, and as the strength of rock is higher than that of concrete, the τ_{peak} of these samples was higher than that of samples with asperities at the front.

These results indicate that a tensile failure, in the asperity or in the concrete, is a possible failure mode for first-order asperity in the concrete-rock interface under eccentric load, especially when the asperity is located at the front or at the end. This failure mode is generally not considered in failure criteria developed for direct shear. Assuming that sliding or shearing of first-order asperity takes place may therefore imply that the shear strength is overestimated.

4.2. Comparison of results with rigid body methods

The SFM and LEM used in the dam safety guidelines suggest using the MC criterion to calculate the available shear strength of the concrete-rock interface. As mentioned in Section 1, the effect of first-order asperity is usually not considered when the FS is calculated with these methods. As an illustrative example, to obtain the magnitude of the potential model discrepancy when first-order asperities are not considered, τ_{peak} values of all the samples were predicted using the MC criterion. The failure plane was assumed as a horizontal plane without any asperity (see Fig. 11). A friction angle of 39.3° was used for calculation, which was obtained from the shear test on samples with planar surfaces. The test results were compared with the predicted values from the rigid body methods (Eqs. (2) and (4)) and the models' discrepancies were calculated as

$$\text{discrepancy} = \frac{-(\text{test} - \text{model})}{\text{test}} \tag{12}$$

A negative model discrepancy indicates that the methods underestimated τ_{peak} while a positive model discrepancy indicates that it overestimated τ_{peak}.

From the comparisons with the direct shear tests, it can be seen that the MC criterion underestimates τ_{peak} for all the locations of the asperity (see Fig. 12a and Table 3). The estimated τ_{peak} for a planar interface without any asperity was about 20%–30% of τ_{peak} from the tests. A model discrepancy of −85% to −70% was obtained for all the samples, irrespective of the location of asperity.

For the eccentric shear tests with an asperity at the front, it can be seen in Fig. 12 and Table 3 that estimated τ_{peak} for a planar interface without any asperity is similar to the τ_{peak} obtained from the test. Thus, the contribution of asperity under these conditions is insignificant. Model discrepancies ranged from −51% to 10%. The model discrepancy of −50% occurred at 0.2 MPa normal pressure. However, the actual discrepancy was just about 0.1 MPa. Due to the small value of τ_{peak}, the model discrepancy seemed greater (see Fig. 12b). At 0.6 MPa and 1.0 MPa of normal pressures, the model discrepancy was 5% and 10%, respectively.

For samples with an asperity in the middle, the estimated τ_{peak} was about 40%–60% of τ_{peak} from the tests. The failure in these tests occurred in concrete. As the concrete is stronger than the planar concrete-rock interface assumed in calculation, the rigid body methods resulted in a model discrepancy between −60% and −40%.

For the samples with an asperity at the end, the estimated τ_{peak} was about 25%–35% of τ_{peak} from the tests. For these samples, the observed failure mode was failure through the rock asperity, resulting in a model discrepancy of −65% to −75%.

To sum up, these results show that sliding stability assessment of concrete-rock interface without considering the first-order asperity is conservative and does not capture the true strength of the interface.

4.3. Implication for dam safety

When evaluating the sliding stability of a concrete dam performed with rigid body methods as suggested in the current dam

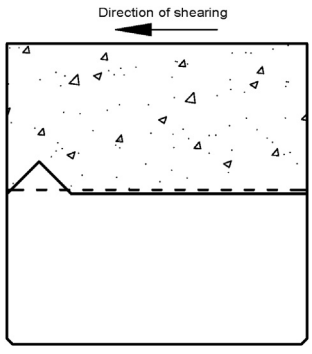

Fig. 11. Assumed failure plane (dotted line in the figure) for sample with asperity at the end.

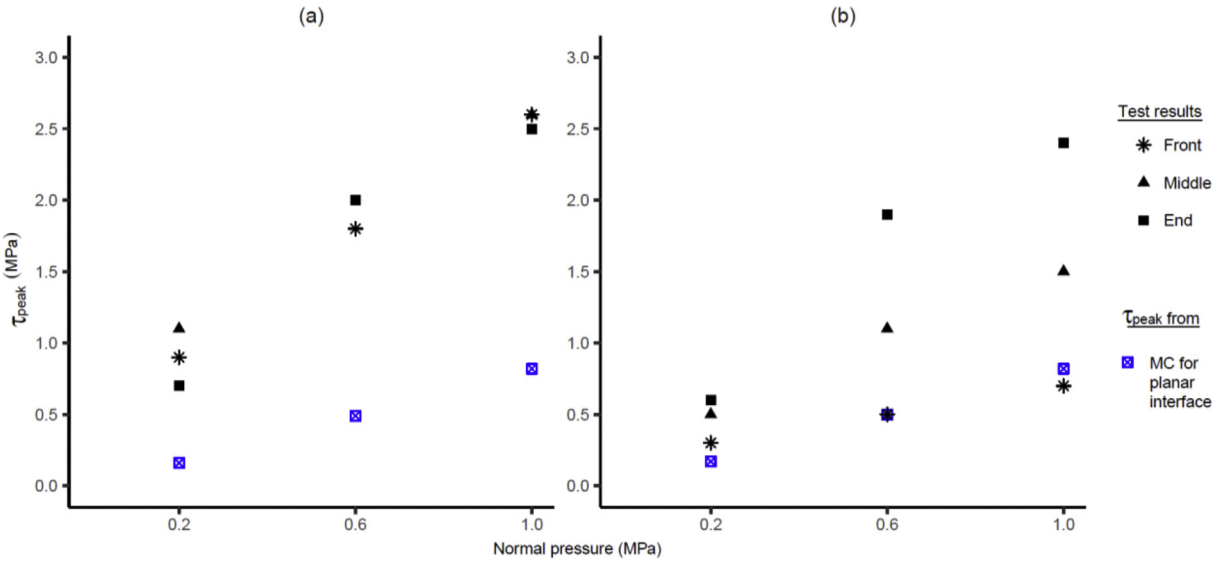

Fig. 12. Comparison of test results with estimated τ_{peak} from MC criterion for a planar interface: (a) Direct shear tests, and (b) Eccentric shear tests.

Table 3
Model discrepancies calculated from the MC criterion.

Sample	Discrepancy (%)	Sample	Discrepancy (%)
DF0.2	−82	EF0.2	−51
DF0.6	−73	EF0.6	5
DF1	−69	EF1	10
DM0.2	−85	EM0.2	−64
DM0.6		EM0.6	−56
DM1	−69	EM1	−43
DE0.2	−77	EE0.2	−71
DE0.6	−75	EE0.6	−74
DE1	−67	EE1	−65

safety guidelines, the FS requirement may not be satisfied for the concrete-rock interface. One reason for this may be that the contribution from large-scale asperity presented on the interface is not considered. Furthermore, the shear test performed under eccentric load in this study clearly shows that the available shear strength may increase if these asperities are considered, thus increasing the FS against sliding. This could avoid unnecessary strengthening of existing dams. However, it shall be noticed that since the laboratory tests were performed under unsaturated conditions, this conclusion is mainly valid for thin-section buttress dams. For these types of dams, the pore water pressure under the buttress will not build up in the same way as that under the concrete gravity dams, since water can be drained to the surroundings. Further studies are required to clarify how saturated condition and uplift pressure influence the contribution of the asperities to the shear strength of gravity dams.

The results from the eccentric shear tests in this study show that under the effect of an eccentric shear force, a tensile failure may be induced in the asperities, which might result in lower shear strength than that obtained by simply assuming a sliding or shear failure of the asperity. Hence, the existing shear criteria were mainly derived for direct shear conditions, without considering all the potential failure modes. This might overestimate the available shear strength and put the dam at risk.

For accurate estimate of τ_{peak} of a concrete-rock interface under eccentric load, the large-scale asperity needs to be considered. The use of simple analytical rigid body methods might not be sufficient and could result in either underestimate or overestimate of the available τ_{peak}. To account for the contribution of first-order asperity in the interface, the principles of fracture mechanics and numerical methods could be applied, taking into account both the location and stress distribution on the first-order asperity. However, further research is required to analyse the capacity of these methods to predict the τ_{peak} for the concrete-rock interface including asperities.

When interpreting these results, it should be noted that this study was limited to an interface with a single asperity at an angle of 45°. An asperity throughout the thickness of the dam was also used in this study. In real dams, this condition is typical for buttresses of buttress dams. For gravity dams, however, it is not obvious that an asperity will be throughout the width of the dam monolith. Hence, the results obtained in this study are mainly valid for buttress/gravity dams where the asperity is throughout the section of the analysed monolith and with asperity angles about 45° or higher. Furthermore, the study was limited to the normal stress ranging from 0.2 MPa to 1.0 MPa. Preferably, further studies should be carried out with multiple asperities, asperity with different inclinations and geometries at the interface, and over a broader range of normal stress, since this will reflect the real condition of the interface under concrete dams.

In addition, the tests in this study were performed on unbonded interface. For some dams, bonded or partly bonded interfaces could occur (e.g. Krounis et al., 2017). The degree of bonding condition depends on factors such as the cleaning of the rock surface prior to casting, the local rock mass quality, the location of leakage, and other degradation processes (Krounis et al., 2015). If bonded interface exists, this could contribute to the τ_{peak}. For example, Mouzannar et al. (2017) performed laboratory shear test on natural, rough and bonded concrete-rock interface under low normal load. They observed that the τ_{peak} was mainly due to the brittle failure of bond between concrete and rock. However, it is likely to assume that the bond breaks at small deformation without any failure in the large-scale asperity. Additional deformation after bond breaking will mobilise the shear strength of large-scale asperity.

5. Conclusions

In this study, the effect of location of first-order asperity on the τ_{peak} was investigated by carrying out direct and eccentric load tests

on concrete-rock samples. Peak shear strengths were predicted using the MC criterion that is commonly used in the SFM and LEM recommended in existing dam safety guidelines as well as with an asperity model. The test results were compared with the predicted shear strength from these analytical models, and model discrepancies were calculated.

In the study, it showed that the location of asperity under eccentric load significantly affects the τ_{peak}. Under the effect of an eccentric shear force, a tensile failure in the asperity or in the concrete is a possible failure mode, especially when the asperity is located towards the front or the end of the interface. This contradicts the assumption of sliding or shear failure in asperity in the existing shear criteria developed for direct shear. The results show that a tensile failure of the rock asperity, or a failure in the concrete, could result in lower shear strength than that obtained by assuming a sliding or shear failure of the asperity.

The results imply that the sliding stability assessment of the concrete-rock interface with rigid body methods or LEM, without considering the first-order asperity, is conservative and does not capture the true strength of the interface. Furthermore, the existing shear criteria to account for first-order asperity are mainly derived for direct shear condition and used for evaluating sliding stability of dams without considering all the potential failure modes. This might overestimate the available shear strength and put the dam at risk. Since the laboratory tests in this study were performed under unsaturated conditions, the conclusions were mainly valid for thin-section buttress dams. Further studies are required to clarify how saturated condition and uplift pressure influence the contribution of the asperity to the shear strength of gravity dams.

Declaration of Competing Interest

The authors wish to confirm that there are no known conflicts of interest associated with this publication and there has been no significant financial support for this work that could have influenced its outcome.

Acknowledgments

This research has been carried out under the project 'Stable Dams'. This project has been funded by the Research Council of Norway (Grant No. 244029). The authors would like to thank Mr. Bård Arntsen at SINTEF Narvik As for his suggestions in planning the laboratory work.

List of symbols

A	Area of failure plane (m^2)
c	Cohesion (Pa)
c_i	Cohesion of intact rock (Pa)
FS_{LEM}	Factor of safety with LEM
FS_{LEM}	Factor of safety with SFM
h	Eccentricity of shear load (m)
I	Moment of inertia (m^4)
i	Angle of asperity (°)
L_{asp}	Length of asperity (m)
N	Normal load (N)
T	Available shear capacity (N)
T_{shear}	Peak shear load for shear failure of asperity (N)
$T_{sliding}$	Peak shear load for sliding failure over the asperity (N)
$T_{tensile}$	Peak shear load for tensile failure of asperity (N)
w	Width of the asperity (m)
$\sum H$	Sum of all shear forces (N)
$\sum N'$	Sum of all normal loads (N)
$\sum M$	Sum of moments (N m)
α	Average inclination of large-scale asperity (°)
σ_c	Compressive stress due to normal load (Pa)
σ_{ci}	Uniaxial compressive strength of rock (Pa)
σ'_n	Effective normal stress (Pa)
σ_t	Tensile stress due to shear load (Pa)
σ_{ti}	Tensile strength of rock (Pa)
τ_{peak}	Peak shear strength (Pa)
τ	Shear stress required for equilibrium (Pa)
τ_R	Available shear stress (Pa)
ε_1	Major strain
ϕ	Friction angle (°)
ϕ_b	Basic friction angle (°)
ϕ_i	Angle of internal friction (°)

References

Altarejos-García L, Escuder-Bueno I, Morales-Torres A. Advances on the failure analysis of the dam-foundation interface of concrete dams. Materials 2015;8(12). https://doi.org/10.3390/ma8125442.

ANCOLD. Guidelines on design criteria for concrete gravity dams. Australian National Committee on Large Dams; 1991.

Asadi MS, Rasouli V, Barla G. A laboratory shear cell used for simulation of shear strength and asperity degradation of rough rock fractures. Rock Mechanics and Rock Engineering 2013;46:683–99.

ASTM D7012-14. Standard test methods for compressive strength and elastic moduli of intact rock core specimens under varying states of stress and temperatures. ASTM International; 2014.

ASTM D3967-16. Standard test method for splitting tensile strength of intact rock core specimens. ASTM International; 2016.

ASTM C39/C39M-17. Standard test method for compressive strength of cylindrical concrete specimens. ASTM International; 2017.

Barton N, Choubey V. The shear strength of rock joints in theory and practice. Rock Mechanics 1977;10:1–54.

Barton N. Suggested methods for the quantitative description of discontinuities. International Society for Rock Mechanics; 1978. p. 319–68.

Bernier C, Padgett Jamie E, Proulx J, Paultre P. Seismic fragility of concrete gravity dams with spatial variation of angle of friction: case study. Journal of Structural Engineering 2016;142(5):05015002.

Brace W. An extension of the Griffith theory of fracture to rocks. Journal of Geophysical Research 1960;65(10):3477–80.

Brown SR, Scholz CH. Broad bandwidth study of the topography of natural rock surfaces. Journal of Geophysical Research: Solid Earth 1985;90(B14):12575–82.

Canadian Dam Association. Dam safety guidelines 2007. 2013 Edition. Canadian Dam Association; 2013.

CFBR. Recommendations for the justification of the stability of gravity dams. Comité Français des Barrages et Réservoirs (CFBR); 2012.

Den Outer A, Kaashoek JF, Hack HRGK. Difficulties with using continuous fractal theory for discontinuity surfaces. International Journal of Rock Mechanics and Mining Sciences & Geomechanics Abstracts 1995;32(1):3–9.

Donnelly SRR. Assessment of shear resistance for blasted rock foundations. In: Proceedings of the CDA 2007 annual conference. St. John's, NL, Canada: Canadian Dam Association; 2007.

FERC. Engineering guidelines for the evaluation of hydropower projects. Chapter 3: Gravity Dams: Federal Energy Regulatory Commission; 2002.

FERC. Engineering guidelines for the evaluation of hydropower projects. Chapter 3: Gravity Dams: Federal Energy Regulatory Commission; 2017.

Fishman YA. Features of shear failure of brittle materials and concrete structures on rock foundations. International Journal of Rock Mechanics and Mining Sciences 2008;45:976–92.

GOM GmbH. ARAMIS—3D motion and deformation sensor. GOM; 2017a. https://www.gom.com/metrology-systems/aramis.html. [Accessed 18 October 2017].

GOM GmbH. GOM correlate/GOM Snap 2D. 2017. https://www.gom.com/news/latest-news/gom-software-2016.html. [Accessed 18 October 2017].

GOM GmbH. GOM correlate software. 2018. https://www.gom.com/3d-software/gom-correlate.html. [Accessed 6 March 2018].

Grasselli G. Shear strength of rock joints based on quantified surface description. Switzerland: EPF Lausanne; 2001. PhD Thesis.

Grasselli G. Manuel Rocha Medal Recipient. Shear strength of rock joints based on quantified surface description. Rock Mechanics and Rock Engineering 2006;39:295.

Gravel C, Moradian Z, Fathi A, Ballivy G, Rivard P, Quirion M. In situ shear testing of simulated dam concrete-rock interfaces. In: Proceedings of the 13th ISRM international congress of rock mechanics. ISRM: International Society for Rock Mechanics and Rock Engineering; 2015.

Haberfield CM, Johnston IW. A mechanistically-based model for rough rock joints. International Journal of Rock Mechanics and Mining Sciences & Geomechanics Abstracts 1994;31:279–92.

Hencher SR, Richards LR. Assessing the shear strength of rock discontinuities at laboratory and field scales. Rock Mechanics and Rock Engineering 2015;48:883–905.

Huang SL, Oelfke SM, Speck RC. Applicability of fractal characterization and modelling to rock joint profiles. International Journal of Rock Mechanics and Mining Sciences & Geomechanics Abstracts 1992;29(2):89–98.
ICOLD. Sliding safety of existing gravity dams. Final report. ICOLD European Club; 2004.
IS. Criteria for design of solid gravity dams. IS: 6512-2003. New Delhi: Bureau of Indian Standards; 2003.
Johansson F. Shear strength of unfilled and rough rock joints in sliding stability analyses of concrete dams. Stockholm: Royal Institute of Technology; 2009.
Johansson F, Stille H. A conceptual model for the peak shear strength of fresh and unweathered rock joints. International Journal of Rock Mechanics and Mining Sciences 2014;69:31–8.
Krounis A, Johansson F, Larsson S. Effects of spatial variation in cohesion over the concrete-rock interface on dam sliding stability. Journal of Rock Mechanics and Geotechnical Engineering 2015;7:659–67.
Krounis A, Johansson F, Larsson S. Shear strength of partially bonded concrete–rock interfaces for application in dam stability analyses. Rock Mechanics and Rock Engineering 2016;49:2711–22.
Krounis A, Johansson F, Spross J, Larsson S. Influence of cohesive strength in probabilistic sliding stability reassessment of concrete dams. Journal of Geotechnical and Geoenvironmental Engineering 2017;143(2):04016094.
Kulatilake PHSW, Shou G, Huang TH, Morgan RM. New peak shear strength criteria for anisotropic rock joints. International Journal of Rock Mechanics and Mining Sciences & Geomechanics Abstracts 1995;32:673–97.
Kulatilake PHSW, Balasingam P, Park J, Morgan R. Natural rock joint roughness quantification through fractal techniques. Geotechnical & Geological Engineering 2006;24(5):1181.
Ladanyi B, Archambault G. Simulation of the shear behaviour of a jointed rock mass. In: Proceedings of the 11th US symposium on rock mechanics; 1970.
Lanaro F, Fredriksson A. Rock mechanics model—summary of the primary data preliminary site description Forsmark area. Report No. 1402-3091. 2005. Sweden.
Li Y, Oh J, Mitra R, Hebblewhite B. A joint asperity degradation model based on the wear process. In: Proceedings of the 49th US rock mechanics/Geomechanics symposium. American Rock Mechanics Association; 2015. p. 8.
Liahagen SA, Lia L, Jørstad O, Sas G. Stabilitet av betongdammer—Ruhetens påvirkning på skjærkapasiteten mellom betong og berg. MSc Thesis. Norwegian University of Science and Technology; 2012 (In Norwegian).
Maksimović M. The shear strength components of a rough rock joint. International Journal of Rock Mechanics and Mining Sciences & Geomechanics Abstracts 1996;33:769–83.
Mouzannar H, Bost M, Leroux M, Virely D. Experimental study of the shear strength of bonded concrete–rock interfaces: surface morphology and scale effect. Rock Mechanics and Rock Engineering 2017;50(10):2601–25.
Muralha J, Grasselli G, Tatone B, Blümel M, Chryssanthakis P, Jiang YJ. ISRM suggested method for laboratory determination of the shear strength of rock joints: revised version. Rock Mechanics and Rock Engineering 2014;47:291–302.
Nicholson GA. Design of gravity dams on rock foundations: sliding stability assessment by limit equilibrium and selection of shear strength parameters. Report No. GL-83-13. Office, Chief of Engineers, U.S. Army; 1983.
NVE. Retningslinjer for betongdammer. The Norwegian water resources and energy directorate. NVE; 2005 (In Norwegian).
Odling NE. Natural fracture profiles, fractal dimension and joint roughness coefficients. Rock Mechanics and Rock Engineering 1994;27(3):135–53.
Oh J, Cording EJ, Moon T. A joint shear model incorporating small-scale and large-scale irregularities. International Journal of Rock Mechanics and Mining Sciences 2015;76:78–87.
Patton FD. Multiple modes of shear failure in rock. In: Proceedings of the 1st international congress of rock mechanics. International Society for Rock Mechanics; 1966.
Plesha ME. Constitutive models for rock discontinuities with dilatancy and surface degradation. International Journal for Numerical and Analytical Methods in Geomechanics 1987;11:345–62.
Schneider H. The friction and deformation behaviour of rock joints. Rock Mechanics 1976;8(3):169–84.
Stowe RL. Strength and deformation properties of granite, basalt, limestone and tuff at various loading rates. US army engineer waterways experiment station. Corps of Engineers; 1969.
USACE. Gravity dam design. US Army Corps of Engineers; 1995.
USACE. Stability analysis of concrete structures. Washington D.C.: US Army Corps of Engineers; 2005.
Wilde MW, Johansson F. System reliability of concrete dams with respect to foundation stability: application to a spillway. Journal of Geotechnical and Geoenvironmental Engineering 2013;139:308–19.
Wilde MW, Johansson F. Probabilistic model code for concrete dams. Stockholm: Energiforsk; 2016.
Xia CC, Tang ZC, Xiao WM, Song YL. New Peak shear strength criterion of rock joints based on quantified surface description. Rock Mechanics and Rock Engineering 2014;47(2):387–400.
Yang J, Rong G, Hou D, Peng J, Zhou C. Experimental study on peak shear strength criterion for rock joints. Rock Mechanics and Rock Engineering 2016;49(3):821–35.
Zhang X, Jiang Q, Chen N, Wei W, Feng X. Laboratory investigation on shear behavior of rock joints and a new peak shear strength criterion. Rock Mechanics and Rock Engineering 2016;49:3495–512.

Mr. Dipen Bista is a PhD candidate at SINTEF Narvik, Norway. He has been working in the field of hydropower for over six years. His research interests are in dam engineering with particular focus on concrete dams. He is currently employed at SINTEF, a leading research institute in Europe.